Document downloaded from:

http://hdl.handle.net/10251/160761

This paper must be cited as:

Martinez-Ortigosa, J.; Simancas-Coloma, J.; Vidal Moya, JA.; Gaveau, P.; Rey Garcia, F.; Alonso, B.; Blasco Lanzuela, T. (2019). Host-Guest and Guest-Guest Interactions of P- and N-Containing Structure Directing Agents Entrapped inside MFI-Type Zeolite by Multinuclear NMR Spectroscopy. The Journal of Physical Chemistry C. 123(36):22324-22334. https://doi.org/10.1021/acs.jpcc.9b05689

The final publication is available at

https://doi.org/10.1021/acs.jpcc.9b05689

Copyright American Chemical Society

Additional Information

"This document is the Accepted Manuscript version of a Published Work that appeared in final form in The Journal of Physical Chemistry C, copyright © American Chemical Society after peer review and technical editing by the publisher. To access the final edited and published work see https://pubs.acs.org/doi/10.1021/acs.jpcc.9b05689".

Host-Guest and Guest-Guest Interactions of P- and N-containing Structure Directing Agents Entrapped Inside MFI-type Zeolite by Multinuclear NMR Spectroscopy

Joaquin Martinez-Ortigosa,¶ Jorge Simancas,¶ J. Alejandro Vidal-Moya,¶ Philippe Gaveau,δ Fernando Rey,¶ Bruno Alonso,δ* Teresa Blasco¶*

¶Instituto de Tecnología Química, Universitat Politècnica de València - Consejo Superior de Investigaciones Científicas (UPV-CSIC), Avda. de los Naranjos s/n, 46022 Valencia, Spain.

δInstitut Charles Gerhardt de Montpellier – UMR 5253 CNRS/UM/ENSCM, 240 avenue du Professeur Emile Jeanbrau, 34296 Montpellier Cedex 5, France.

ABSTRACT: Highly crystalline pure silica MFI zeolites have been synthesized using tetraethylammonium (TEA), tetraethylphosphonium (TEP) or a mixture of both cations in different proportions as organic structure directing agents (OSDAs). The zeolites have been deeply characterized in order to get insight about the guest-guest interactions involving the OSDAs and the guest-host interactions involving the OSDAs and the inorganic framework, as well as the main features of the resulting materials. The results show that the average size of the MFI crystals decreases when TEP is present within the zeolite and that this cation is homogeneously distributed throughout the crystallites. The multinuclear NMR investigation (^{1}H, ^{13}C, ^{14}N, ^{19}F, ^{29}Si, ^{31}P) indicates that TEP interacts with the zeolite host creating higher heterogeneity of the SiO_4 crystallographic sites and a diminution on the mobility of fluorine atoms incorporated into the zeolite. Moreover, the presence of TEP influences the dynamics of the nitrogen atoms of the TEA molecules and 2D heteronuclear correlation experiments give evidence on the spatial proximity of the TEA and TEP molecules in the MFI samples. Then, it is concluded that TEA and TEP are intimately mixed within the zeolites voids of the pure silica MFI samples synthesized by the dual template route using TEP and TEA.

1. INTRODUCTION

Zeolites are crystalline microporous materials with channels and cavities of molecular dimensions that can present a large variety of framework structures and of chemical compositions.[1-2] Most typically, zeolites are silicates or aluminosilicates with varying Si/Al ratios, but they can also contain other atoms such as Ge, Ga, B, Zn, etc. at framework sites. Furthermore, a second wide class of "zeolite" includes microporous aluminophosphate based materials, the so called AlPOs family.[3,4] The most general definition of 'zeolite' is a microporous material with an inorganic 3-dimensional structure composed of fully linked corner-sharing tetrahedral.[5] The diversity of pore systems of zeolite structures and the large range of chemical composition allows tuning their properties making them suitable for large number of industrial applications such as catalysts, membranes, adsorbents, etc.[6-7]

One of the key features of zeolites is the dimensionality and sizes of their channels and cavities that provide them real molecular sieving properties, favoring the diffusion of some compounds or the formation of specific transition states, controlling gas separation and product selectivity in catalytic processes.[8-9] The synthesis of zeolites is usually assisted by using organic molecules, the so called organic structure directing agents (OSDA), generally based on tetraalkylammonium cations, which fill the void volume of the structure and direct the crystallization towards specific topologies.[6,10] The interest in developing new zeolites, mainly aimed at obtaining materials with novel structures, wider chemical compositions and/or modified textural properties has motivated the research on synthesis strategies comprising the use of new OSDA molecules,[9, 11-12] the incorporation of heteroatoms into the framework favoring the crystallization of specific structures (Ge, Zn,…),[13-14] or the dual-template procedure using OSDAs of different nature.[15-16] Moreover, other synthesis variables such as the presence of hydroxyl groups in basic media or F^- in almost neutral gels play a key role on the characteristics of the final material. Fluoride is usually incorporated within the smallest zeolite cages[17,14,18] compensating the positive charge of the OSDAs cations and, in some structures, it bonds silicon atoms giving five-coordinated framework F–SiO_4 sites.[19-20] Synthesis in fluoride media gives crystals free of connectivity defects whereas silanol groups are abundant in the materials synthesized in basic media.

The main features of zeolites (the presence of silanols, the distribution of heteroatoms in the framework, the nature of active sites and its position, the crystal sizes, etc.) are controlled by the preparation procedure.[6,21-22] Accordingly, much research is devoted to the final goal of synthesizing tailored-made zeolites with pore architecture and sites distribution optimized for a particular application.[23] However, despite great research efforts, the synthesis stage remains a mainly experimental field and most of the knowledge acquired along the last decades heavily relies on trial and error even for the most interesting and accessible materials. Therefore, deeper knowledge on the driving forces involved in the zeolite crystallization as well as on the

non-bonding interaction of the OSDA molecules among them and with the inorganic crystalline network is needed for advancing towards the rational design of zeolites synthesis.

In the last years our group has been working on a new family of OSDAs containing phosphorus (P-OSDA) which have shown a great potential for the synthesis of novel zeolites structures, widening the number of available molecules that can be used as directing agents,[12,24-25] but also providing a new characterization tool for understanding the nature of the OSDA entrapped inside of the zeolite voids by means of ^{31}P MAS-NMR. From the point of view of the resulting materials, it is well known that extra-framework phosphorus, which stabilizes framework aluminum against thermal treatment, cannot be introduced in small pore zeolites by post synthesis treatment because of sterical constraints. Recently, an alternative dual-template route with mixtures of P- and N- based OSDAs has been reported for the direct preparation of phosphorous modified small pore zeolites with increased thermal/hydrothermal stability as catalysts for the selective reduction of NO_x and ethanol conversion reactions.[26,27] Then, this synthesis approach expand the potential industrial applications of small pore zeolites by controlling the incorporation of phosphorus.[28-29] For fully exploiting the dual OSDA synthesis route, it is crucial to identify the interactions of the organic cations with the inorganic zeolite host and the properties of the resulting material.

Among the large number of characterization techniques available, MAS NMR spectroscopy is one of the most powerful for the elucidation of the host-guests interactions in zeolites.[30,31] Common NMR nuclei such as ^{29}Si, ^{27}Al and ^{19}F provides information on the inorganic network and ^{13}C on the OSDA occluded in the channels and cavities.[30,32,33] In this work, we expand the usual scope of NMR spectroscopy to ^{31}P and ^{14}N nuclei. ^{31}P MAS-NMR spectroscopy is of relatively straight forward application to P-containing OSDA zeolites because of its high natural abundance and sensitivity. Much more challenging is the NMR studies on ^{14}N (99.6 % natural abundant, $I = 1$) involved in the commonly used tetraalkylammonium directing agents because of its intrinsic low sensitivity (low ^{14}N gyromagnetic ratio) and possible intense quadrupolar interactions.[34] However, it has been shown that tetraalkylammonium cations of relatively high symmetry at the N site give rise to small quadrupolar coupling constants C_Q (<200 kHz) allowing direct acquisition of the ^{14}N NMR signal. It becomes thus possible to investigate the local order in zeolites by inspecting ^{14}N quadrupolar couplings as demonstrated for as-synthesized tetrapropylammonium MFI zeolites with pure silica or aluminosilicate networks.[35,36]

The aim of this work is to get insight into the structure directing properties of mixtures of phosphonium and ammonium based OSDAs, by investigating the interaction between them (guest-guest) and with the inorganic network (host-guest). For this purpose, we have examined pure silica MFI zeolite synthesized in fluoride medium with tetraethylphosphonium (TEP), tetraethylammonium (TEA) or a mixture of them as OSDAs. We have preferred the pure silica modification as a preliminary approach to the more complicated aluminosilicate form. Although the MFI-type is a medium pore zeolite that can be modified with phosphorus by post-synthesis treatment, we have chosen this structure because it can be obtained with large variety of OSDAs broadening the TEA/TEP compositions range that can be used.[15,37-38] The resulting materials have been characterized by various techniques, especially by multinuclear NMR spectroscopy, including ^{31}P and ^{14}N NMR for obtaining direct information on the OSDAs and 2D correlation experiments to get insight on the guest-guest interactions between them and the host-guest interactions with the inorganic framework. Our results allow concluding that the TEA and TEP molecules are intimately mixed within the voids of the same crystals, acting as true co-templates and that the characteristics of the zeolitic material can be modified by combining TEP and TEA as OSDAs.

2. METHODS

2.1. Synthesis of the zeolitic materials

MFI zeolites were synthesized in fluoride media by adding 50 mmol of tetraethylorthosilicate (TEOS; 99%, Aldrich) to an aqueous solution containing 20 mmol of tetraethylammonium (TEA; solution of 35 wt% in water, Aldrich), tetraethylphosphonium (TEP; 98 wt%, ABCR; dissolved in water and exchanged from bromide salt to hydroxide), or a mixture of TEP and TEA. Then, the mixture was stirred until complete hydrolysis of TEOS and evaporation of the necessary amount of water and ethanol, followed by the addition of 20 mmol of HF (48%wt solution in water, Aldrich) in order to obtain a synthesis gel with the following molar composition:

1.0 SiO_2 : 0.4 OSDA : 10 H_2O : 0.4 HF

Where OSDA is TEA, TEP or a mixture of both with TEP/(TEA+TEP) (expressed in **Table 1** as $P/(P+N)_{gel}$) molar ratios of 0.12 and 0.25. The resulting gel was transferred into Teflon lined stainless-steel autoclaves and heated at 448 K at its autogenous pressure under tumbling (60 rpm) for at least 7 days and up to 12 days. The solid was recovered by filtration, washed exhaustively with distilled water and dried at 373 K overnight. **Table 1** summarizes the chemical composition of the synthesis gels and of the final solids. Zeolites synthesized with only TEP or TEA are denoted as P-MFI or N-MFI, respectively, and those obtained with a mixture of OSDAs are named as xP-MFI were x refer to the TEP/(TEA+TEP) (or P/(P+N)) molar ratio in the solid. For the sake of comparison, a MFI zeolite was synthesized in OH^- media following the same procedure, using TEP as organic agent (sample P-MFI-OH).

2.2. Characterization techniques

The powder X-ray diffraction diagrams were obtained employing a PANalytical X´Pert PRO diffractometer equipped with a graphite monochromator, operating at 45 kV and 40 mA, and using Cu Kα radiation (λ = 1.542 Å). The chemical composition of the solids was measured by Inductively Coupled Plasma Optical Emission Spectroscopy (ICP-OES) in a Varian 710-ES device. TG experiments of MFI zeolites were performed on a Mettler Toledo TGA/SDTA851e device heating ca. 5 mg of sample at a rate of 10 K/min up to 1073 K, under a 20 mL/min air stream. Raman spectra were recorded at room temperature using a 785 nm laser excitation on a Renishaw Raman Spectrometer equipped with a CCD detector. The laser power on the sample was 25 mW and 20 acquisitions were taken for each spectrum. FESEM images were taken with a ZEISS ULTRA 55 microscope. The sample powder was deposited in double-sided tape and analyzed without metal covering. The elemental composition and distribution of phosphorus have been determined by using an EDS probe.

Table 1. Chemical composition of synthesized MFI-zeolites.

Sample	Si/OSDA[1]	$[P/(P+N)]_{gel}$[1]	$[P/(P+N)]_{solid}$[1]	wt % P	OSDA/ u.c.[2]	wt % F[3]	F/OSDA[1]
N-MFI	22.0	0	0.00	0.00	4.4	0.94	0.75
0.2P-MFI	22.8	0.12	0.26	0.54	4.2	0.91	0.72
0.4P-MFI	24.2	0.25	0.42	0.86	4.0	1.03	0.83
P-MFI	23.5	1	1.00	1.99	4.1	0.81	0.66
P-MFI-OH	23.7	1	1.00	2.04	4.1	--	--

[1]Expressed as molar ratios. [2]Number of molecules per unit cell ($Si_{96}O_{192}$). [3]Fluorine quantification by ^{19}F MAS-NMR

A Bruker Avance III HD 400 MHz spectrometer was used to record the following MAS-NMR experiments. $^{1}H/^{13}C$ CP NMR at $\nu_0(^{13}C)$ = 100.6 and $\nu_0(^{1}H)$ = 400.1 MHz were carried out on a 4.0 mm probe spinning the sample at 10 kHz, using a ^{1}H $\pi/2$ pulse length of 2.5 µs with spinal proton decoupling, 2 ms as contact time and 3s as recycle delay. ^{1}H NMR spectra at $\nu_0(^{1}H)$ = 400.1 MHz were acquired with a 3.2 mm probe with 20 kHz as a spinning speed, $\pi/2$ pulse length of 2.5 µs and 15 s as recycle delay. ^{1}H 2D NOESY NMR experiments were done using the 2.5 mm probe spinning the sample at 25 kHz, applying a $\pi/2$ pulse length of 3.6 µs, 0.05 s of mixing time and 3s as a recycle delay. ^{31}P NMR measurements at $\nu_0(^{31}P)$ = 161.9 MHz were done using a 3.2 mm probe spinning at 10 kHz using a $\pi/2$ pulse length of 3.7 µs with spinal proton decoupling and recycle delay of 20s. ^{19}F NMR experiments at $\nu_0(^{19}F)$ = 376.5 MHz were acquired with a 3.2 mm probe spinning the sample at 2.5 or 25 kHz, using a $\pi/2$ pulse length of 5.5 µs and 60s recycle delay for quantitative analysis, done by integration of the signals, using an external reference with known amounts of fluorine. ^{29}Si NMR measurements at $\nu_0(^{29}Si)$ = 79.5 MHz were carried out in a 7.0 mm probe with 3.5 µs pulse length corresponding to 60° flip angle, spinal proton decoupling and 180 s as recycle delay. ^{1}H-^{13}C HETCOR NMR spectra were done using a 4 mm probe and spinning the sample at 10 kHz with the experimental conditions described for the $^{1}H/^{13}C$ CP NMR experiments. NMR spectra were referenced to TMS, $CFCl_3$, adamantine, phosphoric acid and water for ^{29}Si, ^{19}F, ^{13}C, ^{31}P and ^{1}H respectively.
An Agilent VNMRS 600 spectrometer was used to record the ^{14}N MAS NMR single pulse spectra at $\nu_0(^{14}N)$ = 43.3 MHz using 9.5 mm rotors spun at different MAS frequencies (ν_{MAS}) so as to precisely determine quadrupolar parameters. RF field strengths ν_{RF} were set to ca. 21 kHz, flip angles to $\pi/4$ (6 µs, bandwidth ~85 kHz) and recycling delays between 0.15 and 0.5 s. These conditions assure an irradiation that is wide enough, and proper longitudinal relaxation. The number of scans was chosen in the 1000-30000 range depending on ν_{MAS} and temperature. The initial FID points contaminated by signal distortion were removed (left shift) such that Fourier Transform started at the top of the first rotational echo maximum. ^{1}H CW decoupling (ν_{RF} ~ 25 kHz) was used during ^{14}N acquisition. ^{14}N NMR chemical shifts were referenced towards solid NH_4Cl spun at 3 kHz. For the magic angle setting, we use the ^{14}N NMR signal of tetramethyl ammonium bromide as standard. All MAS frequencies were stable within 1-2 Hz.
Variable temperature studies were run on the 600 MHz NMR spectrometer by fixing the temperature around the MAS stator (± 1 K) and equilibrating the sample temperature for 15-30 min. From previous experiments, temperature gradients produce small variations (within 5 K) with the MAS conditions used.
Besides, ^{1}H-^{31}P HETCOR NMR spectra ($\nu_0(^{31}P)$ = 242.9 MHz) were recorded on the 600 spectrometer using a 3.2 mm rotor spun at ν_{MAS} = 20 kHz. The HETCOR pulse sequence incorporates a ^{1}H spin-diffusion block like in WISE experiments[39] (90° pulse - mixing time t_m - 90° pulse, after t_1 evolution and before CP). The contact time t_c was set to 3 ms and the recycle delay to 4 s. ^{1}H CW decoupling (ν_{RF} ~ 50 kHz) was applied during acquisition. ^{31}P chemicals shifts were referenced towards phosphoric acid using solid K_2HPO_4 as secondary reference.
NMR spectra were fitted using the freely available *DmFit* software.[40] The ^{14}N quadrupolar interaction is described at the first order (enough for the systems under study). The quadrupolar coupling constant C_Q and the asymmetry parameter η_Q are defined by the principal values V_{ii} of the electric field gradient tensor (EFG) as follows: $C_Q = eQV_{33}/h$ and $\eta_Q = (V_{11} - V_{22})/V_{33}$ where h is Planck's constant, Q the nuclear quadrupolar moment and $|V_{33}| > |V_{22}| > |V_{11}|$.

3. RESULTS

3.1 Characterization of MFI zeolites

The chemical composition of the MFI-zeolites including the TEP/(TEA+TEP) molar ratio, expressed as $[P/(P+N)]_{gel}$ in the synthesis gels and $[P/(P+N)]_{solid}$ in the solid are summarized in **Table 1**. The results indicate that all zeolites, synthesized with TEP, TEA or a mixture of them, contain about 65 mmoles of OSDAs per gram corresponding to about 4 molecules per unit cell. However, the $[P/(P+N)]_{solid}$ in samples prepared in presence of mixtures of P and N-OSDAs (i.e. 0.2P-MFI and 0.4P-MFI) is about double than in the corresponding $[P/(P+N)]_{gel}$, indicating that the incorporation of TEP is favored (**Figure S1**). This result agrees with the increase of the crystallization rate as the P-OSDA content rises (**Figure S2**), although only highly crystalline samples obtained at different crystallization times are considered in this work.
The XRD patterns of all solids, shown in **Figure 1**, are typical of the MFI structure with evident differences in the relative intensity of low angle diffraction peaks, which has been attributed to the different aspect ratio of the MFI zeolite crystals.[41] Indeed, **Figure 2** shows the FESEM images of representative samples that exhibit the coffin crystal shape characteristic of MFI type zeolites with very different crystal sizes and aspect ratios. The average crystal sizes are of about 60 x 10 µm for N-MFI and decrease to 20 x 5 µm for 0.2P-MFI and 0.4P-MFI, while sample P-MFI displays more heterogeneity in the crystal size distribution, with some crystals of smaller size. Chemical composition mapping of phosphorus and silicon in 0.4P-MFI sample,

which was synthesized with TEP and TEA, is shown in **Figure 2**. Several punctual EDX compositional analyses reveal practically the same phosphorus and silicon contents in all the points collected and therefore, these results indicate that P-OSDA is homogenously distributed through the whole MFI crystals.

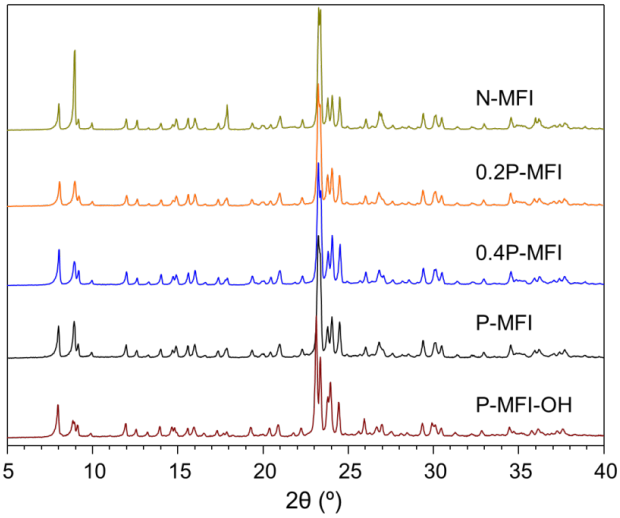

Figure 1. Powder XRD patterns of the as-synthesized MFI zeolites.

Differential thermogravimetric analysis profiles (DTG) of N-MFI and P-MFI show the main weight losses at T ≈ 653 K and at T ≈ 798 K from the decomposition of TEA and TEP, respectively, indicating that the alkylphosphonium is more thermally stable than the ammonium counterpart. The DTG curves of 0.4P-MFI and 0.2P-MFI containing a mixture of OSDAs show two peaks, the one at the lowest temperature is due to the decomposition of TEA, being only slightly shifted towards higher temperatures, whereas that of TEP appears at considerably lower temperature (T ≈ 748 K) (**Figure S3**). These results suggest that the two organic agents coexist as an intimate mixture filling the pores of the MFI zeolites synthesized by the dual OSDA route.

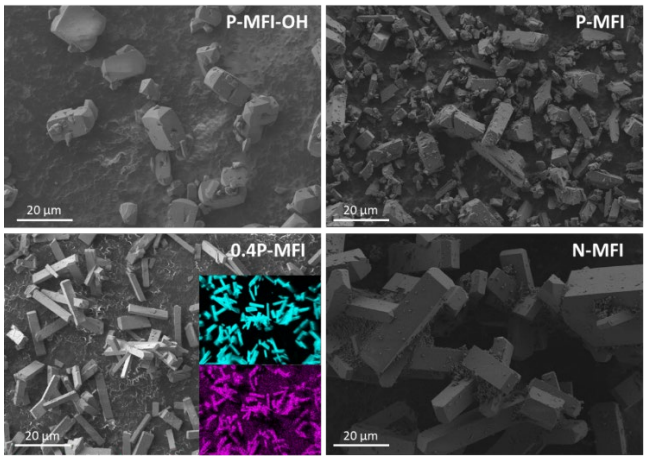

Figure 2. FESEM images of: P-MFI-OH, P-MFI, 0.4P-MFI and N-MFI as-synthesized zeolites. The inset in the image of 0.4P-MFI represents the chemical distribution by EDX of P (pink) and Si (blue).

The TEA molecules within the zeolite voids have been reported to be able to adopt two different conformations depending on the framework topology, which are easily identified by Raman C-N vibration frequencies at ~ 662 cm^{-1} for tg.tg (trans-gauche) and at ~ 672 cm^{-1} for tt.tt (all-trans) conformations that correspond to tetrahedral and disk-like shapes, respectively.[42] The Raman spectrum of the N-MFI zeolite, shown in **Figure 3**, gives a unique band centered at ~ 662 cm^{-1} of the tg.tg conformer in agreement with previous publications,[42] but to our knowledge, there is no report on the P-containing OSDAs. The C-P vibration of the crystalline TEP^+I^- appears at 614 cm^{-1}, while its aqueous solution gives two bands, at 610 cm^{-1} and 590 cm^{-1} (**Figure 3**) which, assuming a behavior similar to that of TEA, can be assigned to the tt.tt and tg.tg conformations, respectively. TEP in the P-MFI and P-MFI-OH zeolites gives a band at 584 cm^{-1} (**Figure 3**) strongly suggesting that, as for TEA, TEP adopts the tg.tg conformation in the MFI zeolite. According to their chemical composition, the spectra of samples 0.2-TEP and 0.4-TEP contain the band at 660 cm^{-1} of the tg.tg conformer of TEA, and a band at 584 cm^{-1} of TEP, tentatively, with a tg.tg conformation.

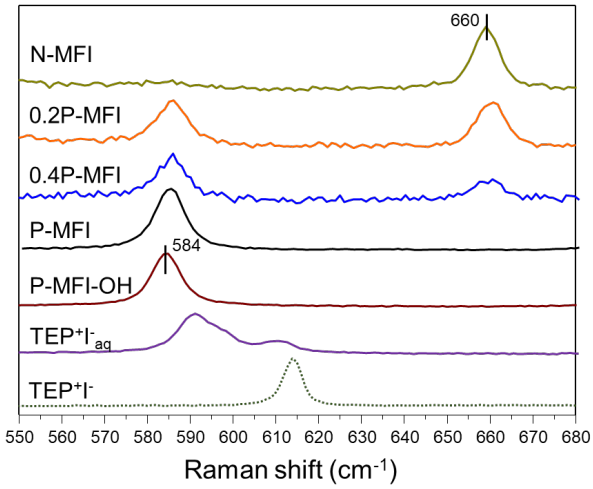

Figure 3. Raman spectra of the as-synthesized MFI zeolites and TEP^+I^- in aqueous solution and in its crystalline form.

Summarizing, the crystallization of pure silica MFI is faster and give smaller crystals when TEP or TEP plus TEA are used as OSDAs. Our results indicate that the incorporation of TEP is more favorable and suggest that TEP and TEA are present in the same crystals acting as real co-templates.

A more exhaustive characterization by means of multinuclear NMR spectroscopy of the MFI zeolites synthesized using P-containing OSDAs has been carried out to get information on the environment of the OSDA molecules (^1H, ^{13}C, ^{14}N, ^{31}P) and the zeolite framework (^{29}Si, ^{19}F) at a local level, for supporting the co-template effect in the characteristic of MFI zeolites

3.2 Solid-state MAS-NMR study

The ^{29}Si NMR spectra of the MFI zeolites are shown in **Figure 4**. The spectrum of N-MFI is well resolved differentiating at simple sight at least nine Q^4 peaks coming from the 12 TO_4 crystallographic sites contained in the MFI topology (*Pnma* spatial group).[43] However, as the relative content of TEP in the samples increases the spectral resolution progressively drops, indicating a distribution of $\delta^{29}Si$ and then higher local disorder. It must be noticed that none of the samples exhibit the typical

doublet of five-coordinated O_4Si–F species at δ ^{29}Si ≈ – 145 ppm due the scalar J coupling of the Si-F bond.[44] Instead, the spectra contain a band at δ ^{29}Si ≈ – 125 ppm, better distinguished for N-MFI and 0.2P-MFI zeolites (see **Figure 4**) due to the exchange between four and five coordinated silicon in the NMR time scale, originated by the mobility of the fluorine that exchange the bonding between two different silicon atoms (the two "mirror related" Si-9) of the $[4^15^26^2]$ cage where it is located.[19,45] The spectrum of P-MFI-OH synthesized in basic medium is the less resolved with an intense and broad band at δ ^{29}Si = – 104 ppm attributed to connectivity defects of Si-O$^-$/Si-OH type. [46,47-48] As expected, this band is hardly detected in the spectra of the samples synthesized in fluoride media with few connectivity defects. The band of Si-O$^-$/Si-OH defects (δ ^{29}Si = – 104 ppm) is only observed, with weak intensity, in the spectrum of the P-MFI zeolite (see **Figure 4**), although it becomes evident in the ^{1}H/^{29}Si-CP experiments (not shown). The higher relative amount of defects can be explained by the lower F/OSDA molar ratio in this sample, which requires more Si-O$^-$/Si-OH defects to compensate the positive charge from the OSDA.

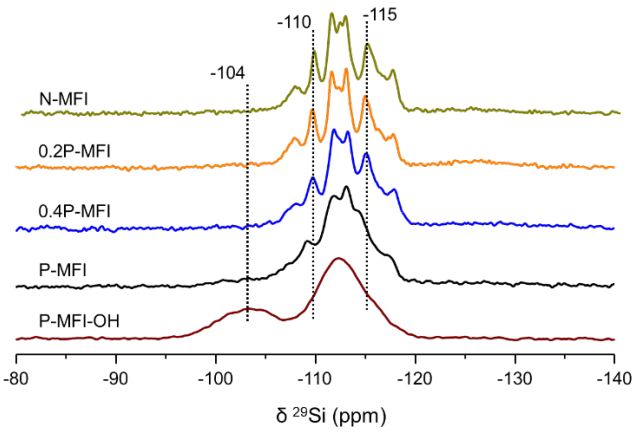

Figure 4. ^{29}Si NMR of the as-synthesized MFI zeolites.

The incorporation of TEA and TEP molecules inside the zeolite channels was investigated by ^{1}H/^{13}C CP (**Figure 5**) and single pulse ^{31}P (**Figure 6b**), and the counter-balancing fluorine atoms by ^{19}F (**Figure 6a**) MAS NMR spectroscopy. The ^{1}H/^{13}C CP NMR spectrum of the P-MFI zeolite consists of two signals at δ ^{13}C = 4 ppm for –**C**H$_3$ and δ ^{13}C = 12 ppm for P–**C**H$_2$– from the ethyl groups of the $[P(–\mathbf{C}H_2–\mathbf{C}H_3)_4]^+$ (TEP). Inspection of the peak at δ ^{13}C = 12 ppm reveals a doublet due to the ^{13}C and ^{31}P scalar coupling with J_{CP} ≈ 30-35 Hz. The N-MFI zeolite also gives two signals at δ ^{13}C = 6 and δ ^{13}C = 54 ppm for –**C**H$_3$ and N–**C**H$_2$–, respectively, from the ethyl group of the $[N(–\mathbf{C}H_2–\mathbf{C}H_3)_4]^+$ (TEA). The ^{1}H/^{13}C CP NMR spectra of the zeolites synthesized by the dual template route contain four signals from the ethyl groups, two from TEA and two more from TEP. The fact that the ethyl groups of TEA and TEP in the MFI samples give no extra peaks or shoulder in any sample suggests that the four ethyl groups of the TEA and TEP remains equivalent, in agreement with the observation by Raman spectroscopy of only one type of molecular conformation inside the zeolite. This result contrasts with the ^{13}C NMR spectra reported in the bibliography for pure silica MFI zeolites synthesized using tetraalkylammonium with longer chains (including tetrapropylammonium), which show a loss of equivalency of the alkyl chains depending if they are oriented towards the straight or the sinusoidal channels.[30,32,35] It must be noticed that the ^{13}C spectrum of the P-MFI-OH sample contains broader peaks being the J_{CP} doublet unresolved, in agreement with the higher concentration of silanol defects and the site heterogeneity of Si sites at the local level.

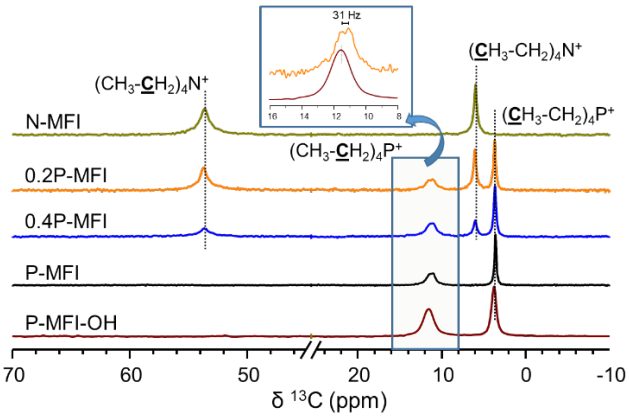

Figure 5. ^{1}H/^{13}C CP MAS NMR over as-synthesized MFI zeolites.

The ^{19}F and ^{31}P MAS-NMR spectra of the MFI materials are shown in **Figure 6**. The ^{19}F spectra of the zeolite samples give an asymmetric signal at δ ^{19}F ≈ – 64 ppm for N-MFI, which progressively broaden and shifts to high field as the TEP content in the sample increases up to δ ^{19}F ≈ – 66 ppm for P-MFI. This signal is typical of fluorine located within the $[4^15^26^2]$ cages bonded to silicon atoms giving the five coordinated F–SiO_4 units.

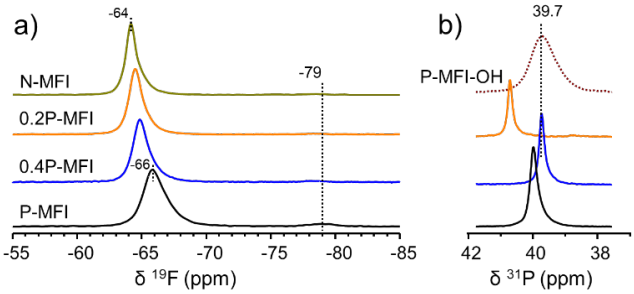

Figure 6. a) ^{19}F and b) ^{31}P MAS-NMR spectra of the as-synthesized MFI zeolites.

Further information on the local symmetry of fluorine is obtained from the simulation of the spectra recorded at low spinning rates containing equally spaced bands separated by the rotating frequency (**Figure 7 and Figure S4**). The contour of the spinning side bands pattern reproduces the shape of the static spectrum providing information on the chemical shift anisotropy (CSA), which is otherwise averaged out at high speed. Fitting of the ^{19}F spectra recorded at rates of ≈ 2.5 kHz, illustrated in **Figure 7** for samples N-MFI and P-MFI,[19] requires at least two components (signals 1 and 2) described by the δ_{iso}, span (Ω), and skew (κ) standard parameters, as well as the asymmetry parameter (η) defined as indicated as a footnote in **Table 2**.[19] The span of signals 1 and 2 are within the range Ω ≈ 45-70 ppm, which according to literature data, indicates reorientation and bonding of fluorine to more than one silicon atom in a dynamic situation. This agrees with the observation of a broad ^{29}Si signal in the range δ ^{29}Si = –120 and –130 ppm, an average of

$^{29}SiO_4$ and $O_4{}^{29}Si–F$ environments, in the spectra of **Figure 4**.[19,45] The Ω of signals 1 and 2 reflects a dynamic state of fluoride intermediate between isotropic motion that would give a symmetric resonance with Ω ≈ 0 and the fix bonding to one silicon atom in a F–SiO_4 site (δ^{29}Si = –140 and –150 ppm) giving more anisotropic ^{19}F signals with Ω ≈ 80-90 ppm. The latter behavior has been reported for spectra recorded at low temperature where the fluoride mobility is frozen.[19] The CSA parameters indicates that the shape of signal 1 (Ω ≈ 46 – 52 ppm, η ≈ 1 and κ ≈ 0) is more symmetric than signal 2 (Ω ≈ 56 – 66 ppm, η ≈ 0.5 – 0.8 and κ ≈ 0.1 – 0.4) (see **Table 2**), which can be explained by a more regular environment and/or more isotropic fluorine motion. The different sign of κ of signals 1 (κ slightly < 0) and 2 (κ > 0) for samples containing TEA reflect differences in the site symmetry of the two signals. It must be mentioned that most of the previous studies on pure silica MFI with TPA as OSDA reported only one ^{19}F NMR signal more similar to signal 1.[19,36]

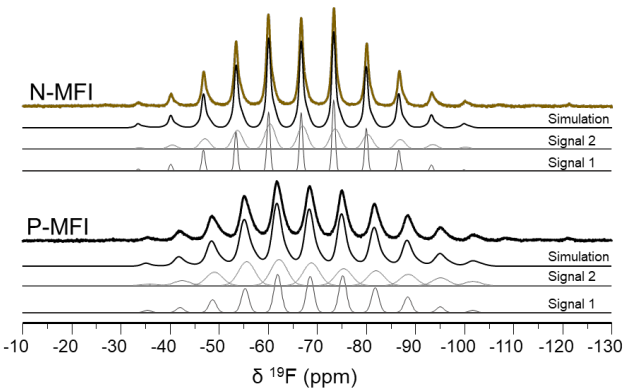

Figure 7. a) ^{19}F CSA spectra of the N-MFI and P-MFI as-synthesized zeolites.

Regarding the evolution of the ^{19}F NMR signals 1 and 2 with the OSDAs, the results reported in **Table 2** show that Ω increases and δ_{iso} ^{19}F progressively shifts to high field as the TEP increases, being these changes slightly larger for signal 2. However, more significant differences are found in the evolution of of κ (and η). The value of κ (and η) of signal 2 change from κ = 0.1 to κ = 0.4 (and η from 0.8 to 0.6) when going from N-MFI to P-MFI, while signal 1 remains practically the same (except for a change of sign of κ in sample P-MFI). These results indicate that the local environment and/or mobility of fluorine giving more asymmetric signal 2 are much more sensitive to the OSDAs than signal 1. Finally, it must be noted that the spectrum of zeolite P-MFI shows a very weak contribution at δ ^{19}F ≈ – 79 ppm, already reported for siliceous MFI and associated to the presence of connectivity defects.[49] The observation of this peak might be related to the higher intensity of the signal of SiO^-/Si-OH in the ^{29}Si NMR spectrum of the P-MFI (see **Figure 4**).

The ^{31}P NMR spectra of samples containing TEP, i.e., 0.2P-MFI, 0.4P-MFI and P-MFI display a single resonance at different positions. Although the δ ^{31}P is not directly correlated with the TEP content in the zeolite, the variation suggests that the phosphorus surrounding is affected by the presence of TEA in the same crystals. It must be noticed that the ^{31}P signal of the P-MFI-OH zeolite is much broader than the P-MFI analogous, with widths at middle height of 150 Hz and 30 Hz, respectively, which must be associated to a higher local heterogeneity originated by the higher content of silanol defects.

Typical ^{14}N NMR spectra of as-synthesized 0.4P-MFI, 0.2P-MFI and N-MFI zeolites recorded at low MAS frequency and at room temperature (≈ 295 K) are presented in **Figure 8**. A single spinning side band pattern (SSB) originating from the ^{14}N quadrupolar interaction can be fitted with a single set of quadrupolar parameters, the quadrupolar coupling constant C_Q and the quadrupolar asymmetry η_Q (**Figure S5**) estimated by using at least three slightly different MAS frequencies. The results obtained differ for the three samples indicating that the defined environment around the ^{14}N site of TEA depends on the relative proportion of TEP within the zeolite. According to previous studies on tetraalkylammonium cations,[34] changes in the quadrupolar interaction and the related Electric Field Gradient (EFG) at the ^{14}N nucleus are originated by modifications on: i) the electron densities around N atom, ii) the distribution of charges in the solid[50] and iii) the mobility of the OSDA molecules. Changes in the electron density at the N atom produced by strong conformational deviations of the OSDAs among the MFI samples studied here (*vide supra*) can be ruled out by the results obtained by Raman spectroscopy, although slight modifications in C–N–C angles cannot be excluded. Second, the distribution of charges in the MFI framework, originating from interactions between TEA, TEP and F^- ions, are not expected to vary significantly among the samples considering the XRD, ^{19}F and ^{31}P NMR results. Regarding the third main cause of modification of the ^{14}N quadrupolar parameters, the motions of the tetraalkylammonium cations,[51] the characteristic timescale of the quadrupolar interaction (10^{-5}-10^{-4} s) is much larger than those of various internal motions. Here, since TEA is smaller (about 33 % in volume) than the tetrapropylammonium cation, the more efficient OSDA for MFI zeolites, the mobility can strongly affect the ^{14}N quadrupolar parameters. Indeed, C_Q values for the ^{14}N of the TEA within the zeolites under study (in the 14-16 kHz range) are significantly lower than that estimated for tetraethylammonium bromide (63 kHz) or earlier for TPA within MFI (50-60 kHz).[35] A simple geometrical model for motions cannot be drawn here and a detailed dynamical analysis is out of the scope of this study. However, some insight on the mobility of the TEA molecules in the presence of TEP in the zeolite, which could explain the difference among the spectra of **Figure 8**, was obtained by recording the ^{14}N spectra at variable temperature.

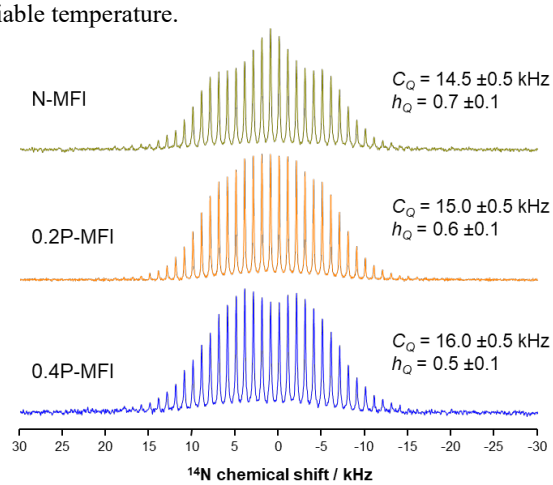

Figure 8. ^{14}N NMR spectra of the 0.4P-MFI, 0.2P-MFI and N-MFI as-synthesized zeolites.

Table 2. ^{19}F MAS-NMR CSA measurements, 2.5 kHz as spinning speed.

		Chemical Shift Anisotropy Calculations									
		Signal 1					Signal 2				
	δiso (ppm)	δ_{ii} (ppm)	δiso_1 (ppm)	Ω (ppm)	η	K	δ_{ii} (ppm)	δiso_2 (ppm)	Ω (ppm)	η	K
N-MFI	-64.3	-40.5 -65.6 -86.8	-64.3	46.2	1.00	-0.08	-37.5 -62.4 -94.1	-64.6	56.6	0.84	0.12
0.2P-MFI	-65.2	-40.9 -66.8 -87.9	-65.2	47.0	1.00	-0.10	-38.2 -62.9 -95.7	-65.6	57.5	0.82	0.14
0.4P-MFI	-65.5	-41.6 -66.2 -88.9	-65.6	47.5	1.00	-0.04	-39.1 -61.1 -98.1	-66.3	59.0	0.69	0.26
P-MFI	-65.9	-40.3 -65.0 -92.5	-65.9	52.2	0.93	0.06	-38.8 -59.6 -104.5	-67.6	65.6	0.56	0.37

*Calculated from the ^{19}F NMR (2.5 kHz) spectra. $\delta_{iso} = (\delta_{11} + \delta_{22} + \delta_{33})/3$; $\delta_{ii} = \delta_{11} \geq \delta_{22} \geq \delta_{33}$; $\Omega = \delta_{11} - \delta_{33}$; $\kappa = 3\,(\delta_{33} - \delta_{iso})/\Omega$ and $\eta = (\delta_{22} - \delta_{11})/(\delta_{33} - \delta_{iso})$.

^{14}N MAS-NMR spectra of zeolites 0.4P-MFI and N-MFI were recorded at temperatures incremented from 230 ±5 K to 360 ±5 K (**Figure S6**). C_Q and η_Q values estimated by spectrum fitting are plotted as a function of temperature in **Figure 9** along with the variations in the effective transverse relaxation time T_2*. Two temperature ranges can be distinguished. The first one runs from 230 K to a transition temperature T' at ≈ 280 K for 0.4P-MFI and ≈300 K for N-MFI. In this T range C_Q and T_2* values gradually decrease and increase, respectively, with temperature. This behavior is consistent with an increase in vibrational and rotational motions leading to an efficient time averaging of the quadrupolar interaction over the different local environments. It is to note that the ^{14}N spectra recorded at the lowest temperatures ($T \approx 230$ K) are more difficult to fit accurately and can reflect a local disorder due to distributions of quadrupolar couplings not averaged out by motions.

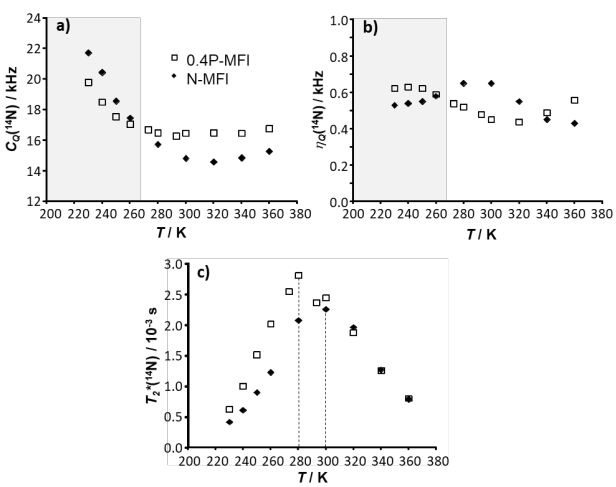

Figure 9. Variation of ^{14}N NMR parameters as a function of temperature: a) quadrupolar coupling constant C_Q, b) quadrupolar asymmetry parameter η_Q, c) effective transverse relaxation time T_2*.

The second temperature range starts at T' and ends at the highest temperature employed ($T \approx 360$ K), the C_Q values are almost constant but T_2* values gradually decrease with temperature while an increase in transverse relaxation times would be expected. This trend, not observed for TPA in all-silica MFI zeolite, is more complicated to explain and we hypothesize that restricted translation motions might be invoked. Interestingly, differences are observed between the C_Q and η_Q values in the two zeolites in the higher temperature range; C_Q is slightly smaller for N-MFI and η_Q follows an opposite trend. Therefore, the results reported in **Figure 9** allows concluding that there is a clear influence of the presence of TEP in the zeolite, which affects the motions of the TEA molecules, possibly in an indirect fashion through geometrical variations of the zeolite framework, and hence the ^{14}N time-averaged quadrupolar couplings.

The ^{1}H NMR spectra of all zeolites, shown in **Figure S7**, display three well differentiated regions: i) $\delta\,^{1}$H ≈ 0 – 4 ppm from the hydrogen atoms of the ethyl groups ii) a very weak signal at $\delta\,^{1}$H ≈ 5 ppm from water, probably within the pores and/or physisorbed, and iii) $\delta\,^{1}$H ≈ 10 ppm of hydrogen bonding silanol groups. The –C**H**$_3$ group of TEP and TEA give signals at $\delta\,^{1}$H = 1.4 ppm and $\delta\,^{1}$H = 1.5 ppm, respectively, the –C**H**$_2$–P at $\delta\,^{1}$H = 2.4 ppm and the –C**H**$_2$–N at $\delta\,^{1}$H = 3.4 ppm. The –C**H**$_2$–P signal is poorly resolved even in P-MFI zeolite. The spectra of **Figure S7** allow distinguishing two main resonances from the ethyl groups; a broad one with maximum at $\delta\,^{1}$H ≈ 1.5 ppm containing signals from all ^{1}H of TEP (–C**H**$_3$ and –C**H**$_2$–P) and from the –C**H**$_3$ of TEA, and a second one at $\delta\,^{1}$H = 3.4 ppm from the –C**H**$_2$–N of TEA. The resonance at $\delta\,^{1}$H ≈ 10 ppm correspond to a silanol nest assembly (Si-O$^-$···HO-Si) containing a siloxy (Si-O$^-$) group that compensates the positive charges of the OSDA in zeolites synthesized in basic media, or balance the fluoride deficiency when the synthesis is carried out in the presence of HF. The exact nature of this defect type is still a matter of debate, being associated to the creation of a silicon vacancy or to hydrolysis of two Si-O-Si bonds to give a siloxy and three silanol groups.[46,48] The signal at $\delta\,^{1}$H ≈ 10 ppm is intense in the P-MFI-OH and very weak in the samples synthesized in fluoride media, because OSDAs' charges are compensated by fluoride anions.

In order to know more about the interaction between TEA and TEP in the samples synthesized by the dual template route, ^{1}H-^{13}C HETCOR **(Figure S8)**, ^{1}H-^{31}P HETCOR (**Figure 10**) and ^{1}H NOESY (**Figure 11**) 2D NMR experiments were performed.

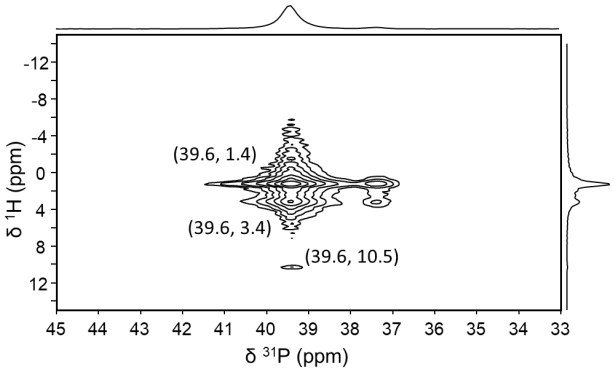

Figure 10. 2D ^{1}H-^{31}P HETCOR-spin diffusion (τ_m = 100 ms) NMR experiment over the as-synthesized 0.4P-MFI zeolite.

The 2D ^{1}H-^{13}C HETCOR NMR spectra, shown in **Figure S8** for the 0.4P-MFI zeolite, give cross-peaks that indicate correlated, spatially close ^{13}C and ^{1}H nuclei. As expected, the spectrum recorded with a relatively small contact time (2 ms) only contains signals of the ethyl groups of TEP (–CH_3 (3.6, 1.4) and –CH_2–P (11.0, 2.4) ppm) and TEA (–CH_3 (5.9, 1.5) and –CH_2–N (53.5, 3.4) ppm), but no cross-peaks correlating TEA and TEP are observed. However, more interesting results are obtained when introducing ^{1}H spin diffusion. The 2D ^{1}H-^{31}P HECTOR spectrum recorded with spin diffusion (τ_m = 100 ms), which is shown in **Figure 10**.

The spectrum contains ^{1}H-^{31}P cross-peaks related to P atoms spatially close to the –C**H**$_3$ groups of the two OSDAs at (39.6, 1.4), the –C**H**$_2$–**P** of the TEP (39.6, 2.4), and the Si-O**H** species (very weak contribution at 39.6, 10.5). It must be mentioned that this experiment allows also the observation of a minoritary signal at δ ^{31}P ≈ 37.0 ppm, not detected in the 1D experiment. The most relevant result of this experiment is the observation of a ^{1}H-^{31}P cross-peak at (39.6, 3.4) corresponding to a correlation between signals of TEP and TEA (^{31}P of P, and ^{1}H of –C**H**$_2$–N respectively), indicating a spatial proximity of both OSDAs at the ~1-100 nanometer scale probe by ^{1}H spin diffusion.[52]

The ^{1}H 2D NOESY experiment, shown in **Figure 11** for samples P-MFI-OH, P-MFI, 0.4P-MFI and N-MFI, allows determining the ^{1}H signals that arise from spatially close protons. The spectra of P-MFI or P-MFI-OH samples present a broad cross-peak centered at (1.4, 1.4) corresponding to –C**H**$_3$ and –C**H**$_2$–P groups, two other cross-peaks (1.4, 10.2), (10.2, 1.4) correlating alkyl and silanol groups, and a cross-peak (10.2, 10.2) for auto-correlation between silanol groups. Similar results are obtained for the other as-synthesized zeolites. The main difference between the spectra of P-MFI and P-MFI-OH is the high intensity of the auto-correlation peak related of silanol groups in P-MFI-OH. However, even the Si-OH signal is weak in the samples synthesized in fluoride media, its relative intensity increases with the phosphorus content in the sample. It must be noted that the ^{1}H signals of –C**H**$_2$–N (δ ^{1}H = 3.4 ppm) and –C**H**$_3$ (δ ^{1}H = 1.5 ppm) are resolved in the samples with higher TEA content (0.4-MFI and N-MFI) and give cross peaks with silanol groups. The similarity between the spectra of Figures 10c and 10d can be understood by the fact that the 1D ^{1}H spectra (see **Figure S7**) does not allow distinguishing the TEP signals from those of TEA, and in particular the peak at δ ^{1}H = 2.4 ppm of the –C**H**$_2$–P group. These experiments demonstrate that there exists a spatial proximity, on the ~1-100 nanometer scale, between the hydrogen atoms of the ethyl groups of both OSDA molecules and the Si-OH defects of the zeolite network. Besides that, a cross-peak in the ^{1}H 2D NOESY experiments can be observed at around (6.2, 6.2) ppm, which is probably due to the water adsorbed or occluded within the zeolitic material.

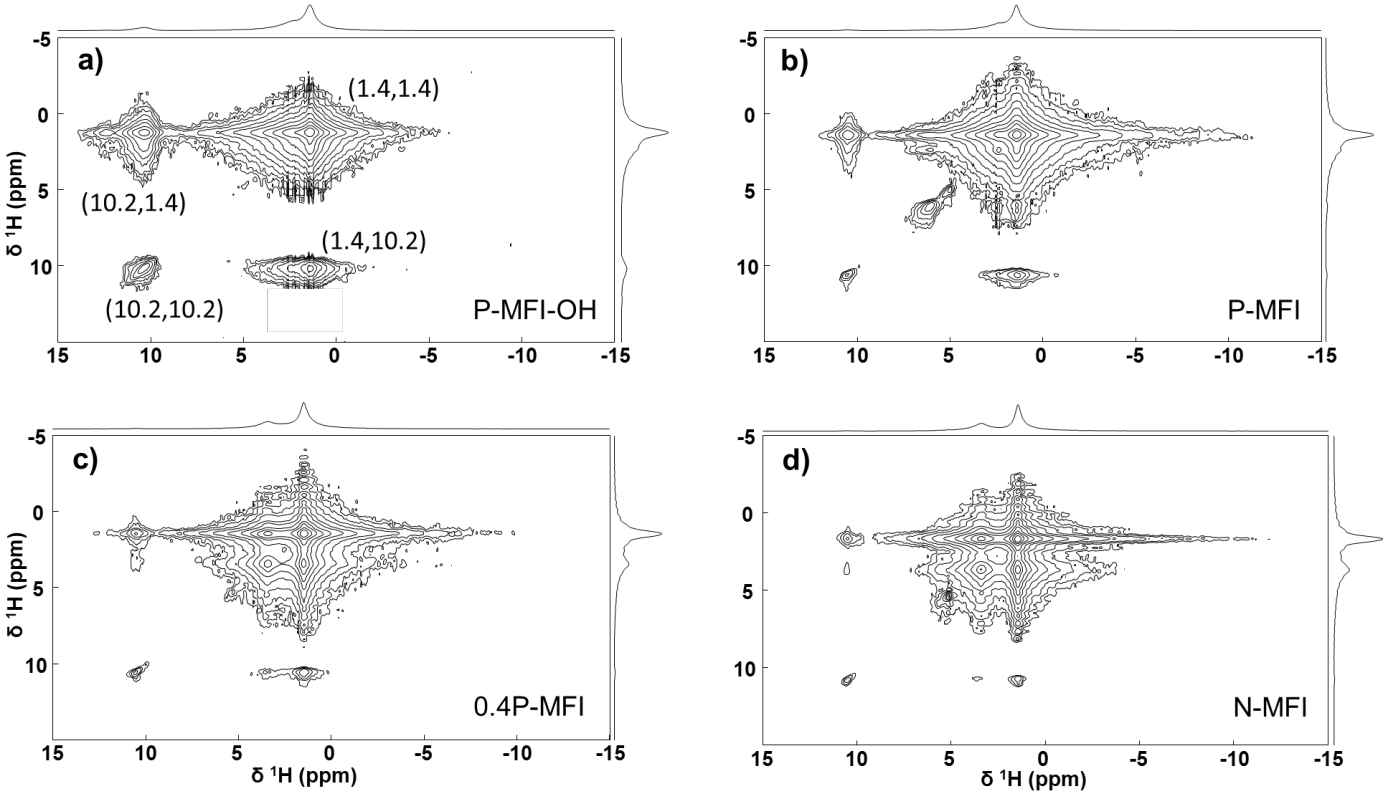

Figure 11. ^{1}H 2D NOESY MAS NMR spectra (t_m = 50 ms) of the as-synthesized zeolites: a) P-MFI-OH, b) P-MFI, c) 0.4-MFI and d) N-MFI.

4. CONCLUSIONS

The use of TEA, TEP or mixtures of both OSDAs has allowed the synthesis of highly crystalline all silica MFI zeolites (silicalite-1). Chemical analysis shows that TEP is favorably incorporated into the material, since the P/(P+N) molar ratio in the recovered solid is always higher than in the synthesis medium, which can explain the shorter crystallization times and the smaller crystal sizes with increasing TEP content. About four molecules of OSDA per unit cell are incorporated in the zeolite, which will be placed at the intersection of straight and sinusoidal channels. Detailed characterization of the MFI zeolites proves that both TEA and TEP are intimately mixed within the voids of the zeolite channels and then that both work as co-structure directing agents.

The multinuclear NMR study indicates that besides the crystallization kinetics, the presence of TEP within the zeolite channels also affects other features of the MFI materials, such as the local structural order and the mobility of the F and N atoms (i.e. Fluoride and TEA species), both of them diminishing as the TEP content increases. The local structural disorder of the SiO_2 framework is directly observed in the ^{29}Si NMR spectra, which show a progressive line broadening as the TEP content in the zeolite increases, being the largest in the P-MFI sample. The widening of the signals reflects the existence of slightly different local geometrical arrangements around the silicon atoms even if placed at the same crystallographic positions. This site heterogeneity may be connected with the occurrence of a minor amount of SiO^- or Si-OH defects that, together with entrapped fluorine, compensate the positively charged OSDA.

The fluorine atoms are incorporated into the MFI structure exhibiting some mobility at room temperature, so that they bond two different Si atoms of the $[4^15^26^2]$ cage in a dynamic way in the NMR timescale. Therefore, the ^{29}Si MAS NMR spectra give a broad band at chemical shifts in between those of tetrahedral $^{29}SiO_4$ and five-coordinated F-$^{29}SiO_4$ geometries. Careful analysis of all ^{19}F NMR spectra allows the identification of a distribution of signals that can be fitted by two superimposed signals. This distribution, which is present in all samples studied in this work including those containing only TEA (N-MFI) or only TEP (P-MFI), is related to variation in the local environment of F. The CSA is not averaged out in the ^{19}F NMR spectra recorded at low spinning rates and the simulation of the corresponding spectra allows the determination of the CSA parameters. According with previous reports relating the span with the mobility,[19,45] the two signals correspond to fluorine species with restricted mobility. The high field signal, less symmetric and with a larger span, corresponds to somewhat less mobile fluorine species, which are more affected by the nature of OSDAs. Its symmetry and mobility further diminish by increasing the TEP content. Meanwhile, the low field signal is only slightly shifted.

The study of the OSDA by Raman spectroscopy indicates that the ethyl chains of occluded organic cations adopt a very similar conformation (probably tg.tg), while the ^{13}C-NMR results show that the ethyl chains are equivalent irrespective its location in the straight or sinusoidal channels of the MFI host, probably because of the relatively small molecular size of ethyl chains. Moreover, it is shown that there is an effect of the relative content in TEP and TEA molecules occluded within the zeolite pores, which is reflected by the variation of δ ^{31}P of the TEP molecules and more especially on the ^{14}N-NMR behavior of the TEA molecules. Temperature dependent ^{14}N quadrupolar parameters are strongly affected by the presence of TEP in the

sample, suggesting that the mobility of the N atoms of TEA is influenced by the presence of TEP in the zeolite. A fully convincing result was obtained by ^{1}H-^{31}P 2D heteronuclear correlation experiment through ^{1}H spin diffusion that unambiguously show the special proximity of P atoms (from TEP) with the hydrogen of the methylene groups of TEA (-C**H**$_2$-N).

The results reported strongly support that the host-guest interactions in pure silica MFI zeolites synthesized with TEA, TEP or mixtures of them depend on the nature of OSDAs present within the zeolite voids. The presence of TEP leads to higher heterogeneity of the SiO_4 crystallographic sites associated to higher local disorder besides some decrease in the mobility of the fluorine atoms. Besides this, our results prove the occurrence of guest-guest interactions between TEP and TEA within the pores of the MFI zeolites synthesized through a dual-template route.

ASSOCIATED CONTENT

Supporting Information.

The TEP/(TEP + TEA) molar ratio in the synthesis gels and in the pure silica MFI zeolites; Crystallization curves of pure silica MFI zeolites; Thermogravimetric analysis of pure silica MFI zeolites; ^{19}F Chemical Shift Anisotropy (CSA) NMR measurements; ^{14}N NMR fitting of the N-MFI, 0.2P-MFI and 0.4P-MFI zeolites; ^{14}N MAS NMR variable temperature study of N-MFI and 0.4P-MFI zeolites; ^{1}H MAS NMR spectra; ^{1}H-^{13}C HETCOR MAS NMR spectrum of the 0.4P-MFI zeolite. This material is available free of charge via the Internet at http://pubs.acs.org.

AUTHOR INFORMATION

Corresponding Author

* Teresa Blasco: tblasco@itq.upv.es
* Bruno Alonso: bruno.alonso@enscm.fr

Notes

The authors declare no competing financial interest.

ACKNOWLEDGMENT

Financial support by the MINECO of Spain through the Severo Ochoa (SEV-2016-0683) and RTI2018-101784-B-I00 projects are gratefully acknowledged. The authors also thank the Microscopy Service of the Universitat Politècnica de València for its assistance in microscopy characterization (FESEM equipment preparation). J.M-O (SEV-2012-0267-02) is grateful to Severo Ochoa Program for a predoctoral fellowship.

REFERENCES

1. Davis, M. E.; Lobo, R. F., Zeolite and Molecular Sieve Synthesis. *Chemistry of Materials* **1992**, *4*, 756-768.
2. Cundy, C. S.; Cox, P. A., The Hydrothermal Synthesis of Zeolites: History and Development from the Earliest Days to the Present Time. *Chemical Reviews* **2003**, *103*, 663-702.
3. Wilson, S. T.; Lok, B. M.; Messina, C. A.; Cannan, T. R.; Flanigen, E. M., Aluminophosphate Molecular Sieves: A New Class of Microporous Crystalline Inorganic Solids. *Journal of the American Chemical Society* **1982**, *104*, 1146-1147.
4. Liu, X.; Yan, N.; Wang, L.; Ma, C.; Guo, P.; Tian, P.; Cao, G.; Liu, Z., Landscape of Alpo-Based Structures and Compositions in the Database of Zeolite Structures. *Microporous and Mesoporous Materials* **2019**, *280*, 105-115.
5. McCusker, L. B.; Liebau, F.; Engelhardt, G., Nomenclature of Structural and Compositional Characteristics of Ordered Microporous and Mesoporous Materials with Inorganic Hosts: (Iupac Recommendations 2001). *Microporous and Mesoporous Materials* **2003**, *58*, 3-13.
6. Davis, M. E., Zeolites from a Materials Chemistry Perspective. *Chemistry of Materials* **2014**, *26*, 239-245.
7. Corma, A.; Martinez, A., Zeolites and Zeotypes as Catalysts. *Advanced Materials* **1995**, *7*, 137-144.
8. Corma, A., From Microporous to Mesoporous Molecular Sieve Materials and Their Use in Catalysis. *Chemical Reviews* **1997**, *97*, 2373-2420.
9. W. Burton, A.; I. Zones, S., *Cheminform Abstract: Organic Molecules in Zeolite Synthesis: Their Preparation and Structure-Directing Effects*, 2010; Vol. 41.
10. Lobo, R. F.; Zones, S. I.; Davis, M. E., Structure-Direction in Zeolite Synthesis. *Journal of inclusion phenomena and molecular recognition in chemistry* **1995**, *21*, 47-78.
11. Moliner, M.; Rey, F.; Corma, A., Towards the Rational Design of Efficient Organic Structure-Directing Agents for Zeolite Synthesis. *Angewandte Chemie International Edition* **2013**, *52*, 13880-13889.
12. Rey, F.; Simancas, J., Beyond Nitrogen Osdas. In *Insights into the Chemistry of Organic Structure-Directing Agents in the Synthesis of Zeolitic Materials*, Gómez-Hortigüela, L., Ed. Springer International Publishing: Cham, 2018; pp 103-138.
13. Martínez, C.; Corma, A., Inorganic Molecular Sieves: Preparation, Modification and Industrial Application in Catalytic Processes. *Coordination Chemistry Reviews* **2011**, *255*, 1558-1580.
14. Sastre, G.; Vidal-Moya, J. A.; Blasco, T.; Rius, J.; Jordá, J. L.; Navarro, M. T.; Rey, F.; Corma, A., Preferential Location of Ge Atoms in Polymorph C of Beta Zeolite (Itq-17) and Their Structure-Directing Effect: A Computational, Xrd, and Nmr Spectroscopic Study. *Angewandte Chemie International Edition* **2002**, *41*, 4722-4726.
15. Chauhan, N. L.; Das, J.; Jasra, R. V.; Parikh, P. A.; Murthy, Z. V. P., Synthesis of Small-Sized Zsm-5 Zeolites Employing Mixed Structure Directing Agents. *Materials Letters* **2012**, *74*, 115-117.
16. Mitani, E.; Yamasaki, Y.; Tsunoji, N.; Sadakane, M.; Sano, T., Synthesis of Phosphorus-Modified Afx Zeolite Using a Dual-Template Method with Tetraethylphosphonium Hydroxide as Phosphorus Modification Agent. *Microporous and Mesoporous Materials* **2018**, *267*, 192-197.
17. Blasco, T.; Corma, A.; Díaz-Cabañas, M. J.; Rey, F.; Vidal-Moya, J. A.; Zicovich-Wilson, C. M., Preferential Location of Ge in the Double Four-Membered Ring Units of Itq-7 Zeolite. *The Journal of Physical Chemistry B* **2002**, *106*, 2634-2642.
18. Camblor, M. A.; Villaescusa, L. A.; Díaz-Cabañas, M. J., Synthesis of All-Silica and High-Silica Molecular Sieves in Fluoride Media. *Topics in Catalysis* **1999**, *9*, 59-76.
19. Koller, H.; Wölker, A.; Villaescusa, L. A.; Díaz-Cabañas, M. J.; Valencia, S.; Camblor, M. A., Five-Coordinate Silicon in High-Silica Zeolites. *Journal of the American Chemical Society* **1999**, *121*, 3368-3376.
20. Koller, H.; Wölker, A.; Eckert, H.; Panz, C.; Behrens, P., Five-Coordinate Silicon in Zeolites: Probing Sio4/2f− Sites in Nonasil and Zsm-5 with 29si Solid-State Nmr Spectroscopy. *Angewandte Chemie International Edition in English* **1997**, *36*, 2823-2825.
21. Dědeček, J.; Tabor, E.; Sklenak, S., Tuning the Aluminum Distribution in Zeolites to Increase Their Performance in Acid-Catalyzed Reactions. *ChemSusChem* **2019**, *12*, 556-576.
22. Li, C.; Vidal-Moya, A.; Miguel, P. J.; Dedecek, J.; Boronat, M.; Corma, A., Selective Introduction of Acid Sites in Different Confined Positions in Zsm-5 and Its Catalytic Implications. *ACS Catalysis* **2018**, *8*, 7688-7697.
23. Gallego, E. M.; Portilla, M. T.; Paris, C.; León-Escamilla, A.; Boronat, M.; Moliner, M.; Corma, A., "Ab Initio" Synthesis of Zeolites for Preestablished Catalytic Reactions. *Science* **2017**, *355*, 1051-1054.
24. Simancas, J.; Simancas, R.; Bereciartua, P. J.; Jorda, J. L.; Rey, F.; Corma, A.; Nicolopoulos, S.; Pratim Das, P.; Gemmi, M.; Mugnaioli, E., Ultrafast Electron Diffraction Tomography for Structure Determination of the New Zeolite Itq-58. *Journal of the American Chemical Society* **2016**, *138*, 10116-10119.

25. Yun, Y.; Hernandez, M.; Wan, W.; Zou, X.; Jorda, J. L.; Cantin, A.; Rey, F.; Corma, A., The First Zeolite with a Tri-Directional Extra-Large 14-Ring Pore System Derived Using a Phosphonium-Based Organic Molecule. *Chemical Communications* **2015**, *51*, 7602-7605.
26. Sonoda, T.; Maruo, T.; Yamasaki, Y.; Tsunoji, N.; Takamitsu, Y.; Sadakane, M.; Sano, T., Synthesis of High-Silica Aei Zeolites with Enhanced Thermal Stability by Hydrothermal Conversion of Fau Zeolites, and Their Activity in the Selective Catalytic Reduction of Nox with Nh3. *Journal of Materials Chemistry A* **2015**, *3*, 857-865.
27. Kakiuchi, Y.; Tanigawa, T.; Tsunoji, N.; Takamitsu, Y.; Sadakane, M.; Sano, T., Phosphorus Modified Small-Pore Zeolites and Their Catalytic Performances in Ethanol Conversion and Nh3-Scr Reactions. *Applied Catalysis A: General* **2019**, *575*, 204-213.
28. van der Bij, H. E.; Weckhuysen, B. M., Phosphorus Promotion and Poisoning in Zeolite-Based Materials: Synthesis, Characterisation and Catalysis. *Chemical Society Reviews* **2015**, *44*, 7406-7428.
29. Blasco, T.; Corma, A.; Martínez-Triguero, J., Hydrothermal Stabilization of Zsm-5 Catalytic-Cracking Additives by Phosphorus Addition. *Journal of Catalysis* **2006**, *237*, 267-277.
30. Liu, X.; Luo, Q., Solid State Nmr Spectroscopy Studies of the Nature of Structure Direction of Osdas in Pure-Silica Zeolites Zsm-5 and Beta. *The Journal of Physical Chemistry C* **2017**, *121*, 13211-13217.
31. Fyfe, C. A.; Brouwer, D. H., Optimization, Standardization, and Testing of a New Nmr Method for the Determination of Zeolite Host−Organic Guest Crystal Structures. *Journal of the American Chemical Society* **2006**, *128*, 11860-11871.
32. Dib, E.; Gimenez, A.; Mineva, T.; Alonso, B., Preferential Orientations of Structure Directing Agents in Zeolites. *Dalton Transactions* **2015**, *44*, 16680-16683.
33. Mafra, L.; Vidal-Moya, J. A.; Blasco, T., Chapter Four - Structural Characterization of Zeolites by Advanced Solid State Nmr Spectroscopic Methods. In *Annual Reports on Nmr Spectroscopy*, Webb, G. A., Ed. Academic Press: 2012; Vol. 77, pp 259-351.
34. Dib, E.; Mineva, T.; Alonso, B., Chapter Three - Recent Advances in 14n Solid-State Nmr. In *Annual Reports on Nmr Spectroscopy*, Webb, G. A., Ed. Academic Press: 2016; Vol. 87, pp 175-235.
35. Dib, E.; Mineva, T.; Gaveau, P.; Alonso, B., 14n Solid-State Nmr: A Sensitive Probe of the Local Order in Zeolites. *Physical Chemistry Chemical Physics* **2013**, *15*, 18349-18352.
36. Dib, E.; Mineva, T.; Gaveau, P.; Véron, E.; Sarou-Kanian, V.; Fayon, F.; Alonso, B., Probing Disorder in Al-Zsm-5 Zeolites by 14n Nmr Spectroscopy. *The Journal of Physical Chemistry C* **2017**, *121*, 15831-15841.
37. Tuel, A.; Ben Taărit, Y.; Naccache, C., Characterization of Ts-1 Synthesized Using Mixtures of Tetrabutyl and Tetraethyl Ammonium Hydroxides. *Zeolites* **1993**, *13*, 454-461.
38. Jian Ding, T. X., Haihong Wu, Mingyuan He, One-Step Post-Synthesis Treatment for Preparing Hydrothermally Stable Hierarchically Porous Zsm-5. *Chinese Journal of Catalysis* **2017**, *38*, 48-57.
39. Schmidt-Rohr, K.; Clauss, J.; Spiess, H. W., Correlation of Structure, Mobility, and Morphological Information in Heterogeneous Polymer Materials by Two-Dimensional Wideline-Separation Nmr Spectroscopy. *Macromolecules* **1992**, *25*, 3273-3277.
40. Massiot, D.; Fayon, F.; Capron, M.; King, I.; Le Calvé, S.; Alonso, B.; Durand, J.-O.; Bujoli, B.; Gan, Z.; Hoatson, G., Modelling One- and Two-Dimensional Solid-State Nmr Spectra. *Magnetic Resonance in Chemistry* **2002**, *40*, 70-76.
41. Chen, X.; Yan, W.; Cao, X.; Yu, J.; Xu, R., Fabrication of Silicalite-1 Crystals with Tunable Aspect Ratios by Microwave-Assisted Solvothermal Synthesis. *Microporous and Mesoporous Materials* **2009**, *119*, 217-222.
42. Schmidt, J. E.; Fu, D.; Deem, M. W.; Weckhuysen, B. M., Template–Framework Interactions in Tetraethylammonium-Directed Zeolite Synthesis. *Angewandte Chemie International Edition* **2016**, *55*, 16044-16048.
43. Ch. Baerlocher and L.B. McCusker, D. o. Z. S. h. w. i.-s. o. d.
44. Fyfe, C. A.; Brouwer, D. H.; Lewis, A. R.; Villaescusa, L. A.; Morris, R. E., Combined Solid State Nmr and X-Ray Diffraction Investigation of the Local Structure of the Five-Coordinate Silicon in Fluoride-Containing as-Synthesized Stf Zeolite. *Journal of the American Chemical Society* **2002**, *124*, 7770-7778.
45. Fyfe, C. A.; Brouwer, D. H.; Lewis, A. R.; Chézeau, J.-M., Location of the Fluoride Ion in Tetrapropylammonium Fluoride Silicalite-1 Determined by 1h/19f/29si Triple Resonance Cp, Redor, and Tedor Nmr Experiments. *Journal of the American Chemical Society* **2001**, *123*, 6882-6891.
46. Brunklaus, G.; Koller, H.; Zones, S. I., Defect Models of as-Made High-Silica Zeolites: Clusters of Hydrogen-Bonds and Their Interaction with the Organic Structure-Directing Agents Determined from 1h Double and Triple Quantum Nmr Spectroscopy. *Angewandte Chemie International Edition* **2016**, *55*, 14459-14463.
47. Koller, H.; Lobo, R. F.; Burkett, S. L.; Davis, M. E., Sio-.Cntdot. .Cntdot. .Cntdot.Hosi Hydrogen Bonds in as-Synthesized High-Silica Zeolites. *The Journal of Physical Chemistry* **1995**, *99*, 12588-12596.
48. Dib, E.; Grand, J.; Mintova, S.; Fernandez, C., Structure-Directing Agent Governs the Location of Silanol Defects in Zeolites. *Chemistry of Materials* **2015**, *27*, 7577-7579.
49. Losch, P.; Pinar, A. B.; Willinger, M. G.; Soukup, K.; Chavan, S.; Vincent, B.; Pale, P.; Louis, B., H-Zsm-5 Zeolite Model Crystals: Structure-Diffusion-Activity Relationship in Methanol-to-Olefins Catalysis. *Journal of Catalysis* **2017**, *345*, 11-23.
50. Dib, E.; Alonso, B.; Mineva, T., Dft-D Study of 14n Nuclear Quadrupolar Interactions in Tetra-N-Alkyl Ammonium Halide Crystals. *The Journal of Physical Chemistry A* **2014**, *118*, 3525-3533.
51. Mineva, T.; Gaveau, P.; Galarneau, A.; Massiot, D.; Alonso, B., 14N: A Sensitive Nmr Probe for the Study of Surfactant–Oxide Interfaces. *The Journal of Physical Chemistry C* **2011**, *115*, 19293-19302.
52. Clauss, J., Schmidt-Rohr, K. and Spiess, H.W., Determination of Domain Sizes in Heterogeneous Polymers by Solid-State NMR. *Acta Polym.* **1993**, 44: 1-17.
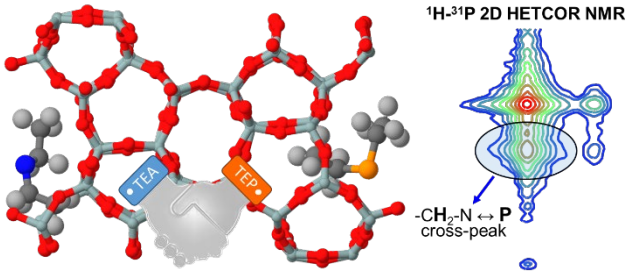
TOC Graphic